UCLouvain

Centre for Cosmology, Particle Physics and Phenomenology

Research Institute in Mathematics and Physics

CR Muons Scattering Simulation Using GEANT4

Project report submitted by

Abhishek
1911007

Date of Submission: 15/07/2023

Supervised by: **Dr.Andrea Giammanco**

Acknowledgements

I would like to express my deepest gratitude to my supervisor Dr Andrea Giammanco for providing this opportunity for this project. I would like to thank Ms Marwa Al Moussawi, for her invaluable support and contributions throughout the completion of this summer project. Their constant guidance, expertise, insightful feedback and encouragement kept me motivated throughout the project. I would also like to extend my sincere gratitude to Prof. Eduardo Cortina Gil, Mr Maxime Lagrange, Mr Ishan Darshana Ran Muthugalalage and Dr Vishal Kumar.

Abstract

This Report presents a comprehensive study on the scattering of cosmic muons using Geant4 and ROOT for simulation and analysis, respectively. A specialized muoscope geometry is designed and employed to simulate the scattering phenomena. The muoscope is capable of differentiating high atomic number (Z) materials by analyzing the spread of scattering angular distributions. The simulation results reveal the intricate interactions between cosmic muons and materials, providing valuable insights into the behaviour of high-energy particles in complex environments. The Point of Closest Approach (POCA) algorithm is also implemented to obtain detailed images of various material cubic blocks, allowing for precise characterization and understanding of their interactions with cosmic muons.Furthermore, to achieve a complete pipeline for muoscope simulation, the integration of Garfield is performed, enhancing the accuracy and efficiency of the simulation process. This work contributes to the advancement of cosmic muon research, opening new ways for exploring materials' properties and enhancing particle detection systems' capabilities.

Table of contents

List of figures

List of tables

Chapter 1

Introduction

1.1   Introduction to Cosmic-Rays Muons

Cosmic rays are high-energy particles that originate from various astrophysical sources, such as supernovae, gamma-ray bursts, and active galactic nuclei. These energetic particles continuously bombard the Earth's atmosphere from outer space. Among the cosmic rays, muons are the secondary particles produced in the upper atmosphere and hold particular significance due to their unique properties and widespread occurrence.

Muons are subatomic particles, similar to electrons, but with a much greater mass. They are lepton types produced in the Earth's atmosphere when cosmic rays interact with air molecules. These secondary muons can penetrate deep into the Earth's surface, reaching depths of several kilometres before they eventually decay into other particles.

Cosmic ray muons carry valuable information about high-energy processes in the universe and provide a means to study fundamental particles and interactions. They are extensively used in various scientific disciplines, including particle physics, geophysics, and astrophysics.

In particle physics experiments, muons serve as a crucial probe for exploring the properties of matter and the fundamental forces that govern the universe. They enable scientists to study the structure of matter at subatomic scales and to search for new particles and phenomena beyond the reach of other experimental techniques

1.2   History of Muons

- **1936: Carl D. Anderson and the Discovery of the Positron:** In 1932, Carl D. Anderson observed the first evidence of the positron, the antimatter counterpart of the electron, while studying cosmic ray interactions in a cloud chamber. This discovery earned him the Nobel Prize in Physics in 1936.

- **1937: Seth Neddermeyer and Cosmic Ray Particles:** While working at Caltech, Seth Neddermeyer and Carl D. Anderson discovered a particle with a mass intermediate between an electron and a proton. Initially, they thought it might be the pion, but later experiments revealed it to be a new type of particle. They named it the "mesotron" (later shortened to "meson").

- **1943: Isidor Rabi and the Muon Name:** In 1943, physicist Isidor Rabi suggested the name "muon" for the newly discovered particle. The term "muon" comes from the Greek letter "mu" (), which is the symbol for the particle's mass. This name helped distinguish the particle from other mesons that were being discovered at the time.

- **1947: Muon Nature and Decays:** By the late 1940s, researchers determined that muons were elementary particles but had a finite lifetime and decayed into other particles. This finding marked the beginning of the exploration of muon properties and interactions.

- **1960s - Present: Muons in Particle Physics:** Muons became essential tools for probing the subatomic world. Particle accelerators, such as the Large Hadron Collider (LHC), have extensively used muons to study high-energy collisions, discover new particles, and test fundamental theories in particle physics.

- **Geophysics and Other Applications:** In the 20th and 21st centuries, muons have found applications beyond particle physics. Muon tomography, a non-destructive imaging technique using cosmic ray muons, has been used to investigate geological structures, archaeological sites, and even the internal composition of volcanoes and pyramids.

1.3 Muons generation in upper atmosphere:

Pions $\left(\pi^+, \pi^0, \pi^-\right)$ and Kaons $\left(K^+, K_S^0, K_L^0, K^-\right)$ are the subnuclear particles most abundantly produced by cosmic rays collision with air molecules in upper atmosphere, and when they are charged their dominant decay modes produce muons : Charged pions ($\pi^\pm$) predominantly decay into muons ($\mu^\pm$) and muon neutrinos (ν_μ or $\bar{\nu}_\mu$) approximately 99.99% of the time. Similarly, charged kaons ($K^\pm$) decay into muons and muon neutrinos about 64% of the time, with an additional 3% of cases involving the production of a π^0 particle. When charged kaons do not directly decay into muons, they mostly decay into two or three pions ($\pi^\pm\pi^0$, $\pi^\pm\pi^\pm\pi^\mp$, or $\pi^\pm\pi^0\pi^0$), and these pions, if charged, can further decay into muons.

The short-lived K_S^0 particle almost always decays into pion pairs ($\pi^+\pi^-$ or $\pi^0\pi^0$). On the other hand, the long-lived K_L^0 particle can decay into pion triplets ($\pi^+\pi^-\pi^0$ or $\pi^0\pi^0\pi^0$). Additionally, K_L^0 produces muons in approximately 27% of its decays through the channel $K_L^0 \rightarrow \pi^\pm\mu^\mp\bar{\nu}_\mu \ (\nu_\mu)$.

These decay processes contribute significantly to the production of muons and other particles in the interactions of cosmic rays with the atmosphere, leading to a diverse range of muon flux observations at the Earth's surface.

1.3.1 Muon Decay

Muon decay is a very short-lived process, with a muon having an average lifetime of about 2.2 microseconds when at rest. Despite this short lifetime, muons originating from cosmic rays manage to reach the Earth's surface due to the effects of special relativity and time dilation.

When muons are created in the upper atmosphere from interactions of high-energy cosmic rays with atmospheric nuclei, they are typically produced with high velocities close to the speed of light (c). As they move at such relativistic speeds, they experience time dilation, a fundamental concept in Einstein's theory of special relativity. Time dilation means time appears to pass more slowly for an object in motion relative to an observer at rest.

Due to time dilation, muons moving at relativistic speeds experience time at a slower rate than an observer at rest on Earth. This means that from the perspective of the muon, its lifetime appears to be longer. As a result, muons can travel much farther than they would if they were at rest before decaying.

The muons have a half-life of 2.2 microseconds. If we assume the speed of muons is approximately close to the speed of light, it would give a range of only 660 m. However, at relativistic speeds, the lifetime of the muon, as we perceive it, is much longer. Given a minimal 2GeV muon (rest mass $= 0.1$GeV): Kinetic Energy :

$$K = amc^2 - mc^2$$

where $a = \frac{1}{\sqrt{1-\frac{u^2}{c^2}}}$ and u is relative velocity rearrange : $a = \frac{K+mc^2}{mc^2} = \frac{(2+0.1)\text{GeV}}{0.1\text{GeV}} = 21$
Using time dilation :

$\Delta t = a\Delta t'$

$\Delta t = 21 \times 2.2 \times 10^{-6}s = 4.6 \times 10^{-s}s$

Range $x = ct$

$$x = \left(3.0 \times 10^2 \text{ m/s}\right) \times \left(4.6 \times 10^{-s}\text{s}\right) = 13860 \text{ m}$$

1.4   Muon Tomography

Muon tomography is a non-invasive imaging technique that uses cosmic ray muons to study the internal structure of various objects or geological formations. The basic principle of muon tomography is similar to medical X-ray or CT (computed tomography) scans but instead uses naturally occurring muons as the probing particles.

- The process of muon tomography involves the following key steps:

- Cosmic Ray Muon Source: Cosmic rays, high-energy particles originating from space, constantly bombard the Earth's atmosphere. Among these cosmic rays, muons are particularly useful for tomography due to their high penetrating power.

- Muon Detectors: Specialized detectors are placed around or near the object being investigated. These detectors are designed to track and record the paths of muons as they pass through the object.

- Muon Absorption and Scattering: As muons pass through the object, their paths may be absorbed or scattered depending on the density and composition of the materials they encounter. Dense materials, such as metals or rock, tend to absorb

more muons, while less dense materials, like air or empty spaces, allow more muons to pass through.

- Data Collection: The detectors continuously collect data on the trajectories of the muons as they pass through the object from various angles.

- Image Reconstruction: By analyzing the collected data, a computer algorithm reconstructs a 3D image or tomogram of the internal structure of the object. The algorithm uses mathematical techniques, such as filtered backprojection or iterative algorithms, to create the image based on the muon absorption and scattering patterns.

Chapter 2

Overview of Muoscope

2.1 Detector Geometry

The Simulated Muoscope detector consists of four parallels planes, each with dimensions of $50 \times 50 \times 0.1\,\mathrm{cm}^3$. The top two planes are designed to store the incoming muon hits, while the bottom two planes store the outgoing muon hits. This arrangement allows for the analysis of the inner structure of the block placed between these planes.

The detector planes are constructed using thin layers of Resistive Plate Chambers (RPC) filled with a gas mixture of 70% Argon and 30% CO2. For the purpose of our analysis, we will assume that the RPCs used in the detector are 100% efficient with infinite resolution, meaning they can detect all muon hits and accurately determine their positions.

In this idealized scenario, when a muon passes through the detector, it will interact with the gas-filled RPC layers, creating ionization tracks along its path. The top two planes will register the positions of these ionization tracks, representing the incoming muon hits. Similarly, as the muon exits the block and passes through the bottom two planes, ionization tracks will be recorded, representing the outgoing muon hits.

By analyzing the positions of the incoming and outgoing muon hits recorded in the detector planes, scientists can reconstruct the trajectory of the muon as it passes through the block. The recorded hits in the detector planes allow researchers to visualize and study the inner structure of the block, identifying any variations in density or material composition within the block.

It is essential to consider that real detectors might have limitations such as finite resolution, inefficiencies, and noise. However, this idealized description provides a starting point for understanding the basic principles of the Muoscoper detector and its potential applications in muon tomography for studying the internal composition of objects.
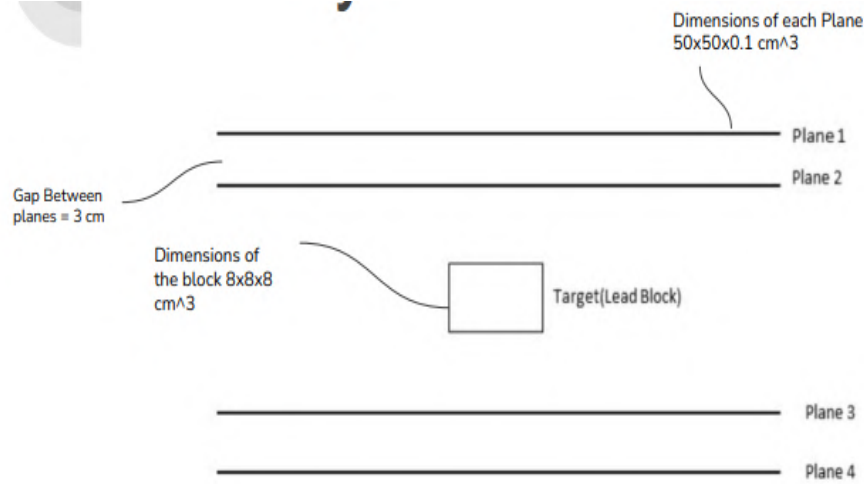

Fig. 2.1 A schematic view muoscope and target.

2.2   Resistive Plate Chamber (RPC)

The active detector component in MuoScope is made up of resistive plate chambers (RPC) [1], which are gaseous parallel-plate detectors with good spatial and time resolution [**?**]. The RPCs used in MuoScope are made up of two glass plates with the dimensions 50cm $\times$ 50 cm $\times$ 1 mm, separated by a 2.5 mm gas gap. These glass plates are coated with graphite which serves as electrodes and a high voltage of around 10 KV is applied. The gas gap is filled with a mixture of R134A (95.5%), isobutane (4.3%), and SF6 (0.2%). But for simplicity, we only used gas planes. 2.2.
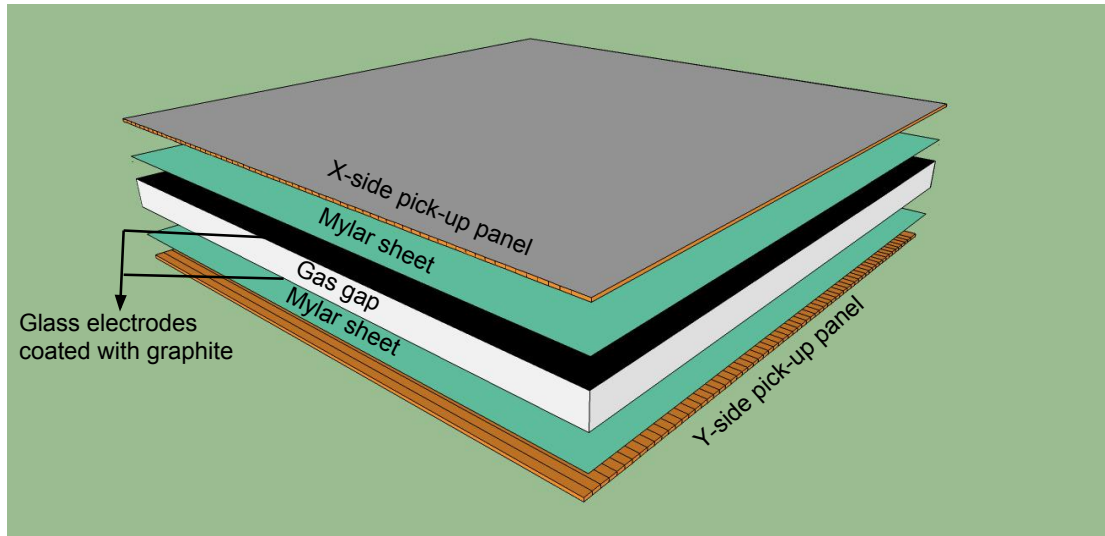
Fig. 2.2 Schematic view of RPC detector showing the orthogonally placed pick-up panels(Note: we did not include this in our geometry.)

Few gas molecules in the RPC get ionised when a muon crosses a detector. The primary electron-ion pairs are accelerated by the strong electric field, which causes further ionisations and the formation of an avalanche. The same is illustrated in figure 2.3.
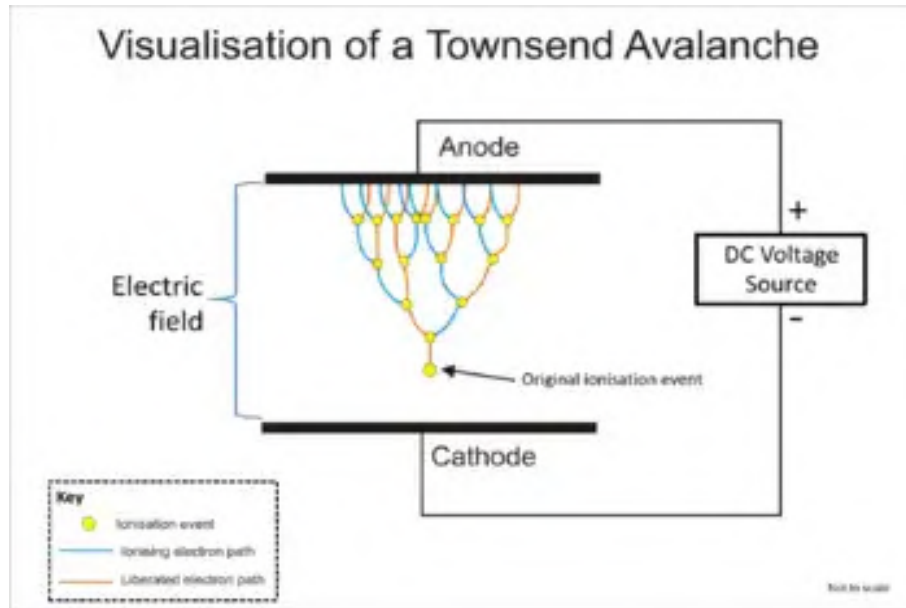
Fig. 2.3 Schematic view of avalanche formation in RPC detector. Ionising radiation triggers an avalanche effect in gas between two plate electrodes, where each ionisation event releases one electron. Subsequent collisions lead to the liberation of additional electrons, resulting in a sustained electron avalanche. (Source: Wiki)

The gas mixture is utilised to regulate the secondary avalanche generation and the avalanche formation is limited to a narrow area of the detector. This charge propagation induces a signal on the pickup panels' readout strips, which gives us the knowledge of the muon's X and Y coordinates in the RPC.

Chapter 3

Muon Interactions

3.1 Muon energy loss

The mean energy loss rate $\left(\text{MeV} \cdot \text{g}^{-1} \cdot \text{cm}^2 \right)$ or mass stopping power(MSP) for a charged particle passing through a medium is given by the Bethe-Bloch formula [54]

$$-\left\langle \frac{dE}{dx} \right\rangle = \frac{4\pi N_A r_e^2 m_e c^2}{A} z^2 \frac{Z}{\beta^2} \left[\frac{1}{2} \ln \frac{2 m_e c^2 \beta^2 \gamma^2 W_{\max}}{I^2} - \beta^2 - \frac{\delta(\beta\gamma)}{2} \right]$$

where, $N_A = 6.02214129(27) \times 10^{23}$ mol^{-1} : Avogadro's number. $r_e = 2.8179403267(27)$fm : Classical electron radius. Z : atomic number of the absorber. A : atomic mass of the absorber $\left(\text{g} \cdot \text{mol}^{-1} \right)$. z : charge number of the incident particle. I : Mean excitation energy (eV). $W_{\max}$: Maximum energy transfer possible in a single collision.

$$W_{\max} = \frac{2 m_e c^2 \beta^2 \gamma^2}{1 + 2\gamma m_e / M + (m_e/M)^2}$$

$m_e c^2$: Electron mass $\left(\text{MeV}/\text{c}^2 \right)$ M : Mass of the incident particle $\left(\text{MeV}/\text{c}^2 \right)$ $\delta(\beta\gamma)$: Density effect correction to ionization energy loss. $\beta = v/c$: where v is the velocity of the particle and c is the speed of light and $\gamma = 1/\sqrt{1-\beta^2}$

3.2 Multiple scattering in materials

Muons travelling through matter experience multiple Coulomb scatterings, which means their paths are deflected due to interactions with atomic nuclei and electrons in

the material. The overall deflection of muons depends on several factors, including the density and atomic number of the material they traverse, the length of the path they travel, and their momentum.

The scattering angle distribution of muons is well-described by Molière's multiple scattering theory. According to this theory, the central 98% of the scattering angle distribution can be approximated by a Gaussian distribution. In other words, the majority of the scattering angles fall within a certain range, and a bell-shaped Gaussian curve closely approximates this range.

The width of the Gaussian distribution represents the spread of scattering angles around the mean value. This width characterizes the extent of scattering experienced by muons as they pass through the material. The broader the width, the more scattering occurs, leading to a larger dispersion of the muon trajectories.

$$\theta_0 = \frac{z \cdot 13.6\text{MeV}}{p\beta c}\sqrt{\frac{x}{X_0}}\left[1 + 0.038 \cdot \ln\left(\frac{x}{X_0}\right)\right]$$

Here, p and βc are the momentum and velocity of the muon, $z = 1$ is the charge of the muon and x and X_0 are the target's thickness and characteristic radiation length, respectively. The radiation length is the mean distance over which an electron loses all but 1/e of its energy and can be written as follows:

$$X_0 = \left[\frac{A \cdot 716.4 \text{ g cm}^{-2}}{Z(Z+1)\ln(287/\sqrt{Z})}\right]\left[\frac{1}{\rho}\right]$$

Here, ρ, A and Z are the material's density, atomic weight and atomic number. The approximate $\rho \cdot Z^2$ dependence for large Z characterises the sensitivity to dense objects with a high atomic number, which is a unique feature of MST. The scattering angle is inversely proportional to the muon momentum.

	Material properties			θ_0 [mrad] at three muon momenta		
	Z	A	ρ [g/cm^3]	0.3 GeV/c	3 GeV/c	30 GeV/c
Acetal	7	14	1.4	19.3	1.8	0.2
Aluminium	13	27	2.7	35.0	3.3	0.3
Silicon	14	28	2.3	34.4	3.2	0.3
Iron	26	56	7.9	83.4	7.9	0.8
Lead	82	207	11.3	156.2	14.7	1.5
Uranium	92	238	19.1	214.5	20.3	2.0

Fig. 3.1 Theoretical scattering angle spread calculated using the above expressions with a thickness of 5cm

In summary, Molière's multiple scattering theory provides a valuable framework for understanding the behaviour of muons as they undergo multiple Coulomb scatterings in matter. The Gaussian approximation of the scattering angle distribution allows scientists to analyze the statistical properties of muon scattering and study the effects of different materials and experimental setups on the overall deflection and trajectory of muons.
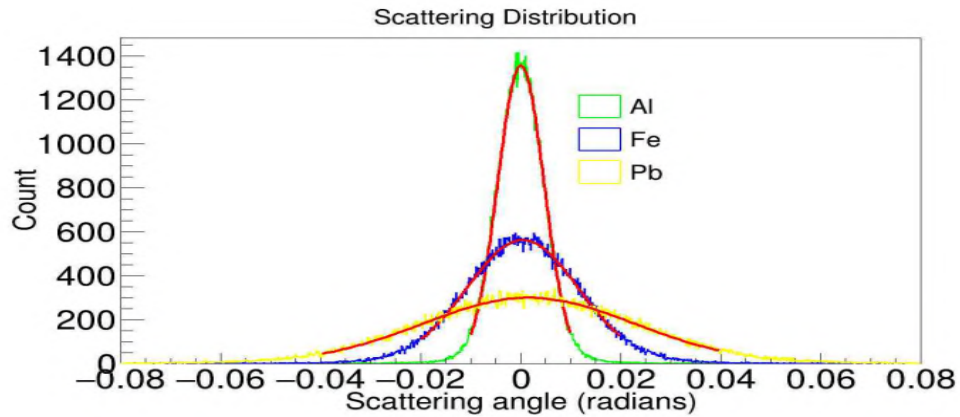

Fig. 3.2 Spread in the distribution is proportional to the value of Z

Chapter 4

Building Geometry

4.1   Simulation Setup

- For building geometry, we used GEANT4 [2] G4VUserDetectorConstruction abstract base class and derived our own class "DetectorConstruction".

- In this class, "DetectorConstruction" a Construct() method was implemented.

- Construct all necessary materials using G4Material. some materials are already available in NIST [3] manager and if it is not we can build it by ourselves for example CO2:   // creating CO2

  G4double a = 12 * g / mole; // carbon
  G4int z;
  G4Element *elC = new G4Element("Carbon", "C", z = 6, a);

  a = 16.00 * g / mole; //
  G4Element *elO = new G4Element("Oxygen", "O", z = 8, a);

  G4double density;
  G4int n;
  G4Material *CO2 = new G4Material("Carbon Dioxide", density = 1.87 * g / cm3, n = 2);
  G4int nAtoms; CO2->AddElement(elC, nAtoms = 1);
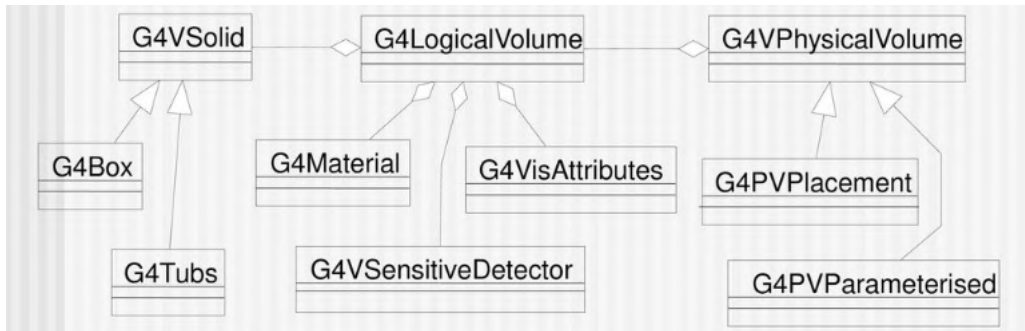 CO2->AddElement(elO, nAtoms = 2);

Fig. 4.1 Basic Strucure for defining working geometry

- In this way we can define several mixtures of gases and test them.

- we have used two mixtures 1. Argon(70%)+CO2(30%) and 2. R134A (95.2%)+Butane(4.5%)+SF6(0.3%)

- Define shapes/solids

- Define logical volumes

- Place volumes of your detector geometry

- Instantiate sensitive detectors / scorers and set them to corresponding volumes (optional)

- Define visualization attributes for the detector elements (optional)
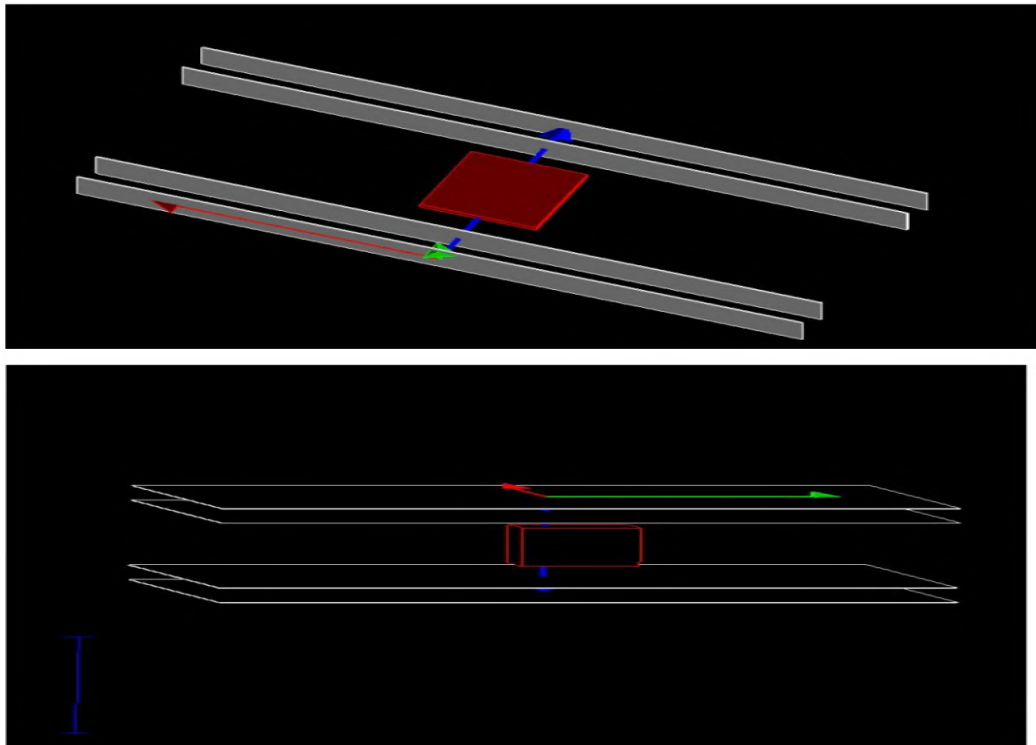
- Define regions (optional)

Fig. 4.2 A simple geometry consisting of four parallel plane and a cubic block

The main components of the geometry are:

- **1a.** Four parallel planes.

- **1b.** A cube placed in between the four planes.

Material Composition:

- **Planes:** 70% Argon + 30% CO_2

- **Cube:** Lead

4.2   Why do we use these gases?

Different gas mixtures are used in RPCs based on their specific requirements. In the case of Argon (70%) and CO2 (30%), Argon provides high ionization efficiency, while CO2 offers a fast response time and helps lower the operating voltage. For other

RPCs like r134a+butane+SF6, each gas contributes specific properties to optimize detector performance. The choice of gas mixtures depends on efficiency, response time, voltage requirements, cost, and safety. Experimental testing determines the optimal combination for each application.

In addition to the properties mentioned earlier, the choice of gas mixtures in RPCs also considers the phenomenon of quenching. Quenching refers to the ability of the gas mixture to stop the electrical discharge once it has been initiated.

In RPCs, electrical discharges occur when ionization electrons created by the passage of particles in the gas accumulate and create a conductive path. If this discharge is not quenched quickly enough, it can lead to continuous discharges, reducing the detector's efficiency and potentially damaging the detector.

The gas mixture's quenching properties play a crucial role in ensuring that the electrical discharge stops promptly after each detection event. This allows the detector to quickly recover and be ready to detect the next particle. The optimal gas mixture should provide effective quenching to maintain the detector's stability and reliability during operation.

Number of RPC	4
Number of Blocks	1
Dimensions of RPC	50 cm × 50 cm × 0.1 cm
Dimensions of Block	8 cm × 8 cm × 8 cm
Gap in between Upper RPCs and lower RPCs	3.5 cm
Gas gap, Pick-up panels, Copper coils, support structures	Not included

Table 4.1 Table summarizing the specifications of simulated geometry.

4.3   Cosmic-Ray Muons Showers using EcoMug

4.3.1   Using Primary Generator

- **Primary Generator:** A primary generator was used to produce 4 GeV muons. The primary generator is a source of high-energy particles that initiates the muon production process.

- **Muon Generation:** Muons are generated from the top of the plane. The muon generation process involves creating muons at the top surface of the specified plane.

- **Random Distribution:** A random distribution is applied for muon generation. This means that muons are produced with random positions and directions within the generator dimension.

- **Generator Dimension:** The dimension of the primary generator is 50×50 cm^2. This defines the area from which muons are produced, and it ensures a uniform coverage of muon generation across the specified plane.

By using a primary generator to produce 4 GeV muons from the top of the 50×50 cm^2 plane with a random distribution, we can simulate a idealistic and basic distribution of muons, essential for studying various properties and interactions in our experimental setup.

Using EcoMug (Efficient COsmic MUon Generator) [4]

1. C++11 header-only library for generating cosmic ray (CR) muons based on experimental data parametrization.
2. Offers various surface options (plane, cylinder, half-sphere) while maintaining accurate angular and momentum distributions.
3. Allows custom differential flux parametrizations for CR muon generation. We used gaisser parametrizations [Gaisser, T.K 1990]

Chapter 5

Data Analysis and Results

5.1 Muon Tomography as an inverse problem

5.2 Tomography

- $\vec{X} \rightarrow$ Input variables for a given dynamical system. Example: Position/direction of a muon at the upper detector. (Known)

- $\vec{f} \rightarrow$ Physics laws governing the evolution of the system. Notice: It can be deterministic but also probabilistic. Example: Moliere's scattering formula for angular deviations. (Known)

- $\vec{\theta} \longrightarrow$ Parameters describing the physics environment. Example: Densities and geometry of the crossed material. (Unknown)

- $\vec{y} \rightarrow$ Output variables after the action of $\vec{f}$. Example: Position/direction of a muon at the lower detector. (known)

Therefore, we can compute $\vec{y} = \vec{f}(\vec{X}; \vec{\theta})$

5.3 Analysis Pipeline

After building the geometry and shooting muons, the following steps were followed to test and store the hits: Generating CR Muons using EcoMug $\longrightarrow$ Storing each

hit in the root file⟶ Analysing the Histograms⟶ Using MakeClass Method to to more rigorous analysis ⟷ imposing required constraint to obtain results ⟷ adding POCA algorithm as a header file.

- **Generating CR muons** First, we used PrimaryGenerator and shot muons of 4GeV using a particle gun, and then using EcoMug, we have generated the CR muons using Flat sky and Gaisser distribution for our flux.
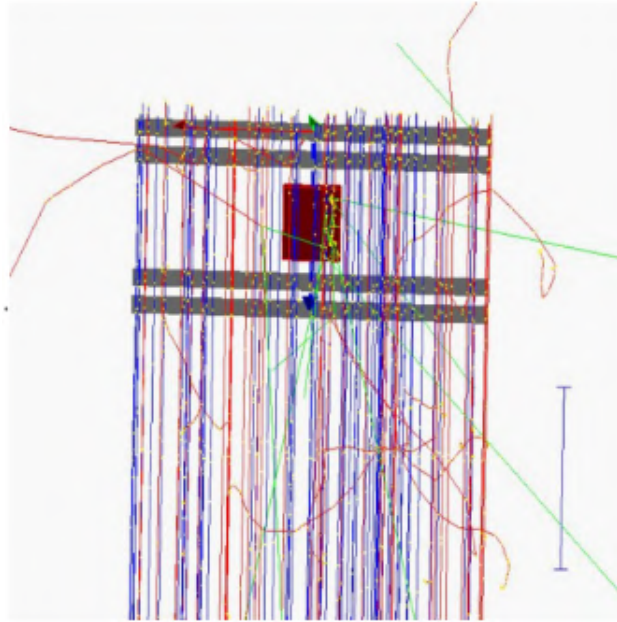

Fig. 5.1 Isortropic and uniform energy muons showers of 4GeV

- **Storing each hit in a ROOT [5] File** We can store hits in a root file, store our data in a histogram, and verify our initial results.

Steps for storing hits in a root file

a) Use the G4AnalysisManager class to produce ROOT output.
b) Create two tuples with specific columns to store the variables generated in the previous. steps. one for storing the hits information and one for storing the Generator information.
c) Filled the tuples with the corresponding variables' values.

Fig. 5.2 We have stored several variables in our root files to verify our initial results.
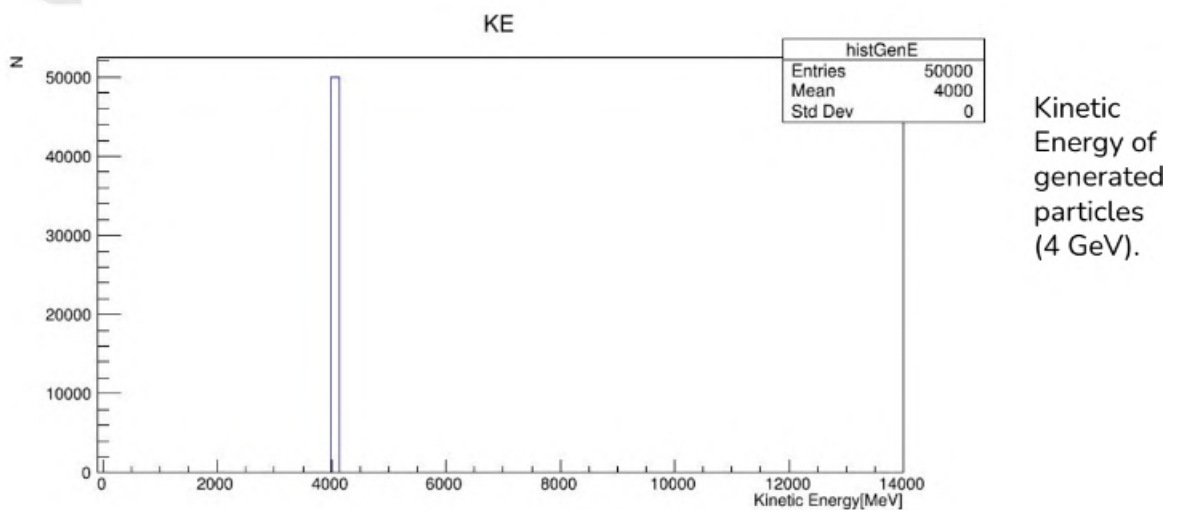

Fig. 5.3 In this histogram we can see that energy is peaking around 4 Gev.

5.4   Energy Loss of cosmic muons in RPC gas

1. We have obtained the energy deposition (Edep) for argon, which agreed with theoretical calculations.

2. Different gas mixtures and material was used:

(A) 70% Argon + 30% CO2 (B) 95.2% R134A +4.5% Butane + 0.3% SF6 .

- (A) 70% Argon + 30% CO2 : Plane thickness: 0.1 cm
  Gas density: 1.80Kg /m3
  Energy loss of muons per unit area of material: $\approx 2MeV/g/cm2$

Total energy loss for the plane:

$$0.1 cm \times 0.00180 g/cm3 \times 2 MeV/g/cm2 \approx 0.00036 MeV$$

- Energy deposition follows the Landau distribution due to multiple scattering, ionization, and the Bethe-Bloch equation. The distribution captures fluctuations in energy loss when high-energy charged particles interact with matter.
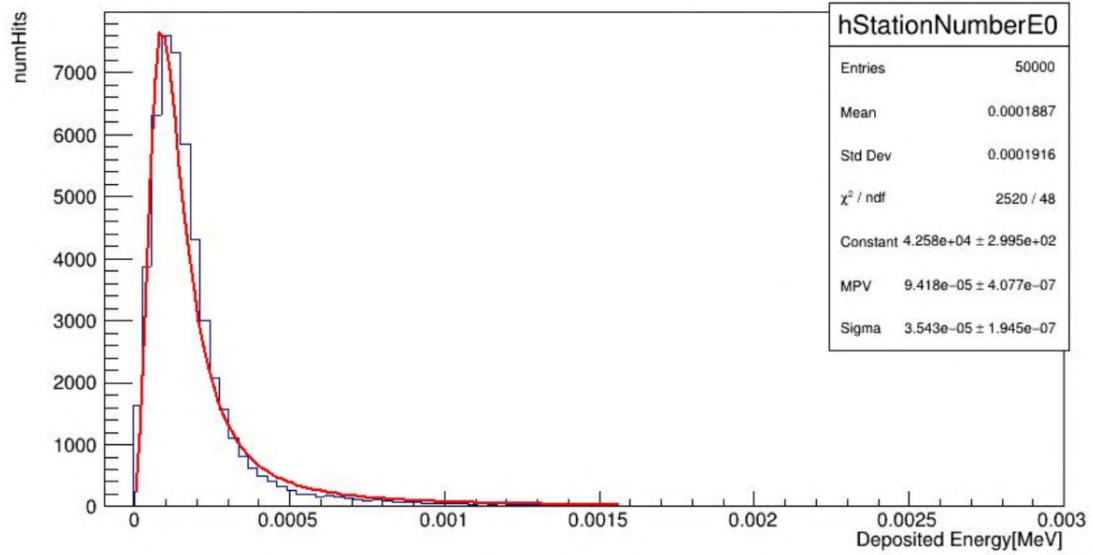
$$f(x; \xi, \lambda) = \frac{1}{\pi} \int_0^\infty e^{-t} \cos\left(\xi t + \frac{x}{\lambda}\right) \frac{dt}{t}$$

Although it is possible to define our landau distribution and fit the obtained energy deposition into this function, it is predefined in the ROOT fit panel.
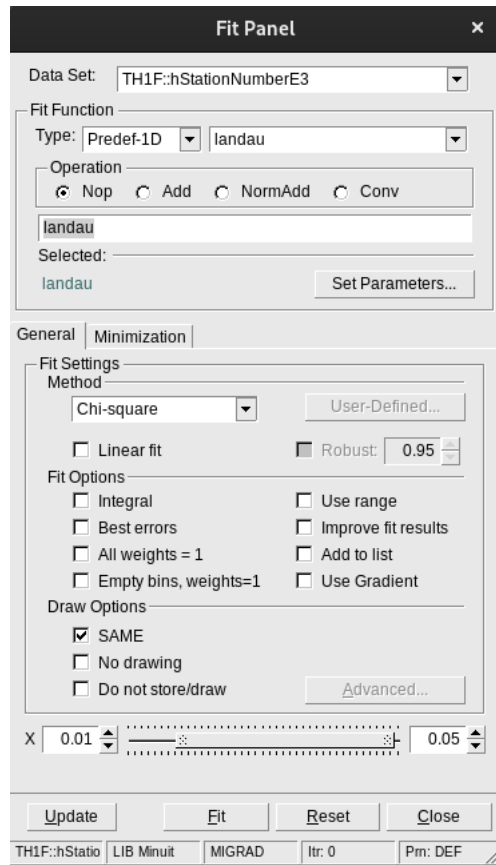
Most probable value (MPV) will be the Edep for obtained energy distribution.

Edep for Argon+CO2 mixture: density (0.00180g /cm3)

hStationNumberE0	
Entries	50000
Mean	0.0001887
Std Dev	0.0001916
χ^2 / ndf	2520 / 48
Constant	4.258e+04 ± 2.995e+02
MPV	9.418e−05 ± 4.077e−07
Sigma	3.543e−05 ± 1.945e−07

- (B) 95.2% R134A +4.5% Butane + 0.3% SF6 : Plane thickness: 0.1 cm
  Gas density: 0.00418g /cm3
  Energy loss of muons per unit area of material: $\approx 2MeV/g/cm2$
  Total energy loss for the plane:

$$0.1cm \times 0.00418g/cm3 \times 2MeV/g/cm2 \approx 0.000836MeV$$

Edep for 95.2% R134A +4.5% Butane + 0.3% SF6 mixture: density (0.00418g /cm3)
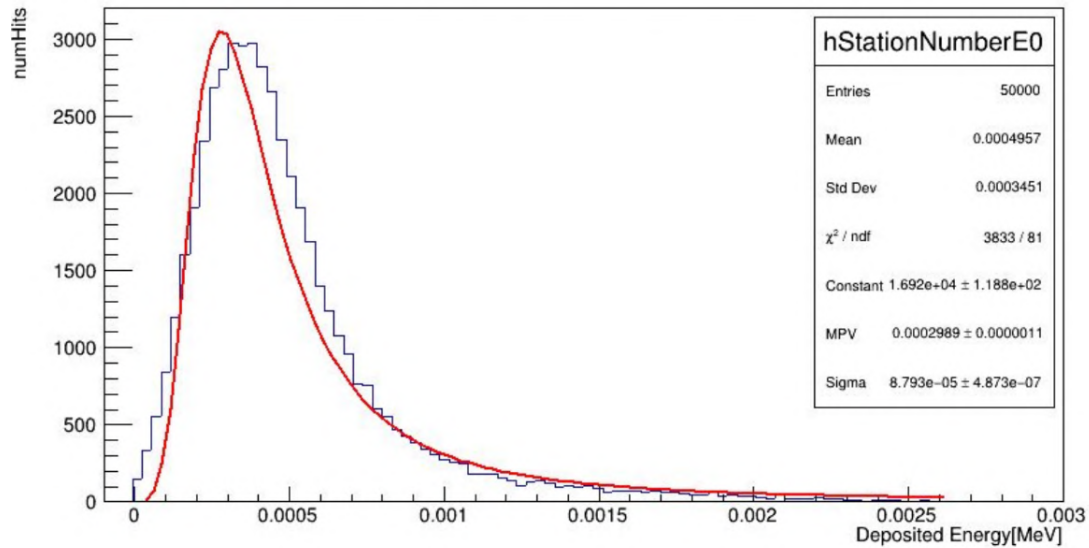
NOTE it is clearly visible that MPV from root fit and theoretical calculations are significantly different. The reason for this difference is we are storing hit per hit. We can find the number of hits per event, and then it would make sense.
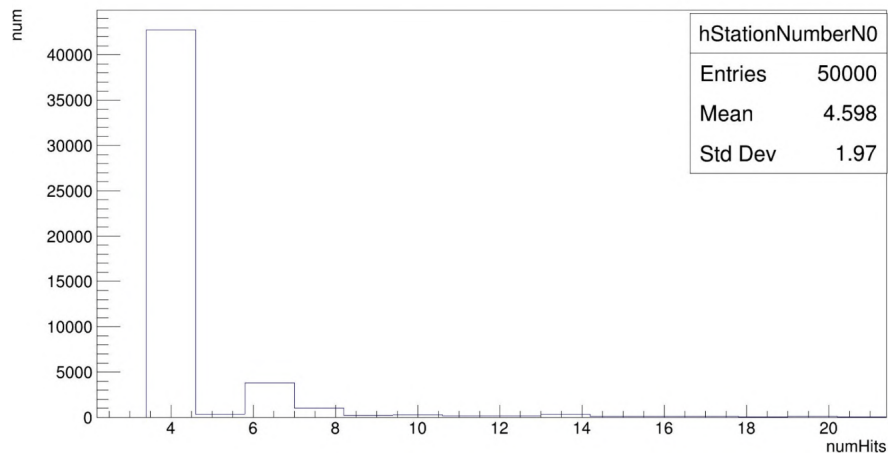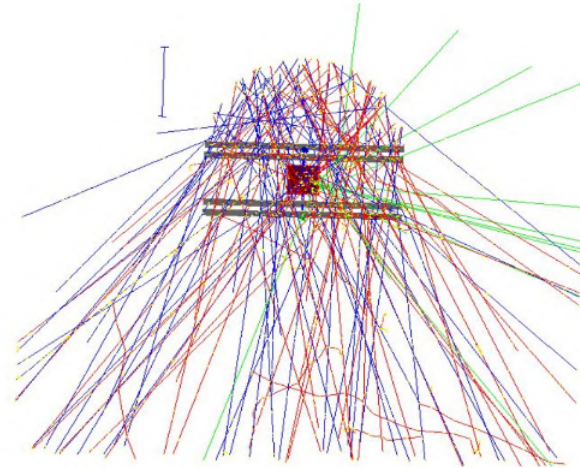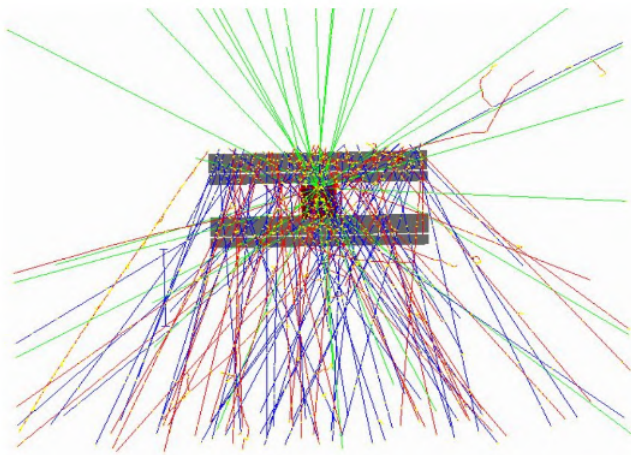
Number of Hits(Geant4 Primary Gen.)

Fig. 5.4 Mean value of num of hits in each event is 4.598. we can multiply this number by MPV.

5.5   Outputs from EcoMuG

**EcoMuG: Flat Sky & Hemispherical surfaces**

We used Flat Sky Surface for our simulations.

In our simulations, we have utilized the Gaisser distribution to model the cosmic muons flux. The Gaisser distribution is an empirical formula used to estimate the differential cosmic muon flux as a function of the muon momentum or energy and the atmospheric depth at which the muons are produced.

```
//....ooo00000ooo........ooo00000ooo........ooo00000oo
double J(double p, double theta) {
double A = 0.14*pow(p, -2.7);
double B = 1. / (1. + 1.1*p*cos(theta)/115.);
double C = 0.054 / (1. + 1.1*p*cos(theta)/850.);
return A*(B+C);
}
```
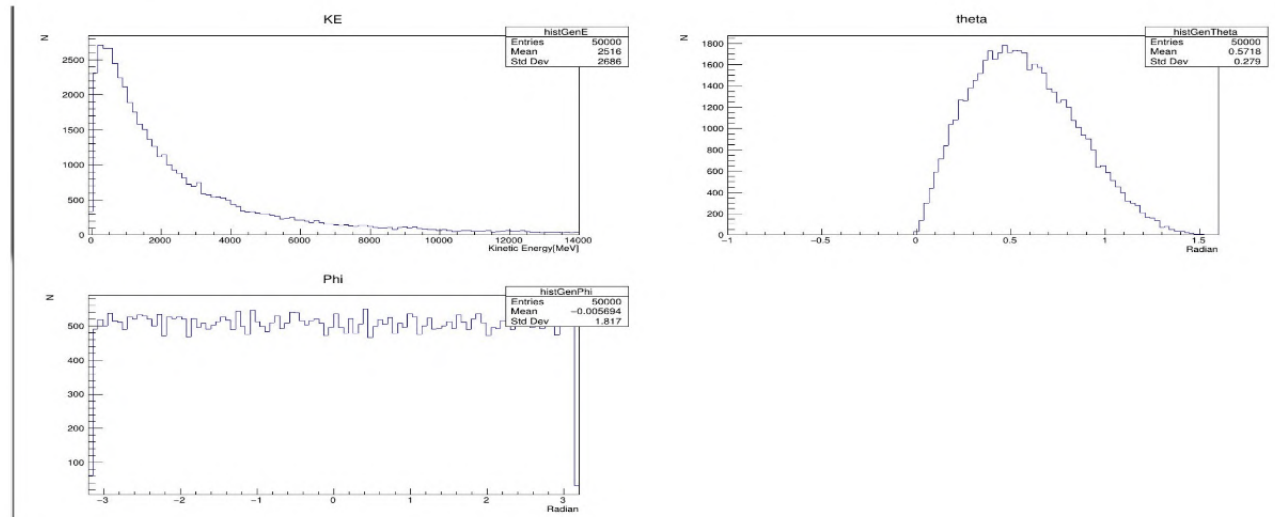
it's not surprising that we obtained the energy distribution as an exponential distribution and the angular distribution (theta) as a cosine square distribution when simulating cosmic muons using the Gaisser distribution.
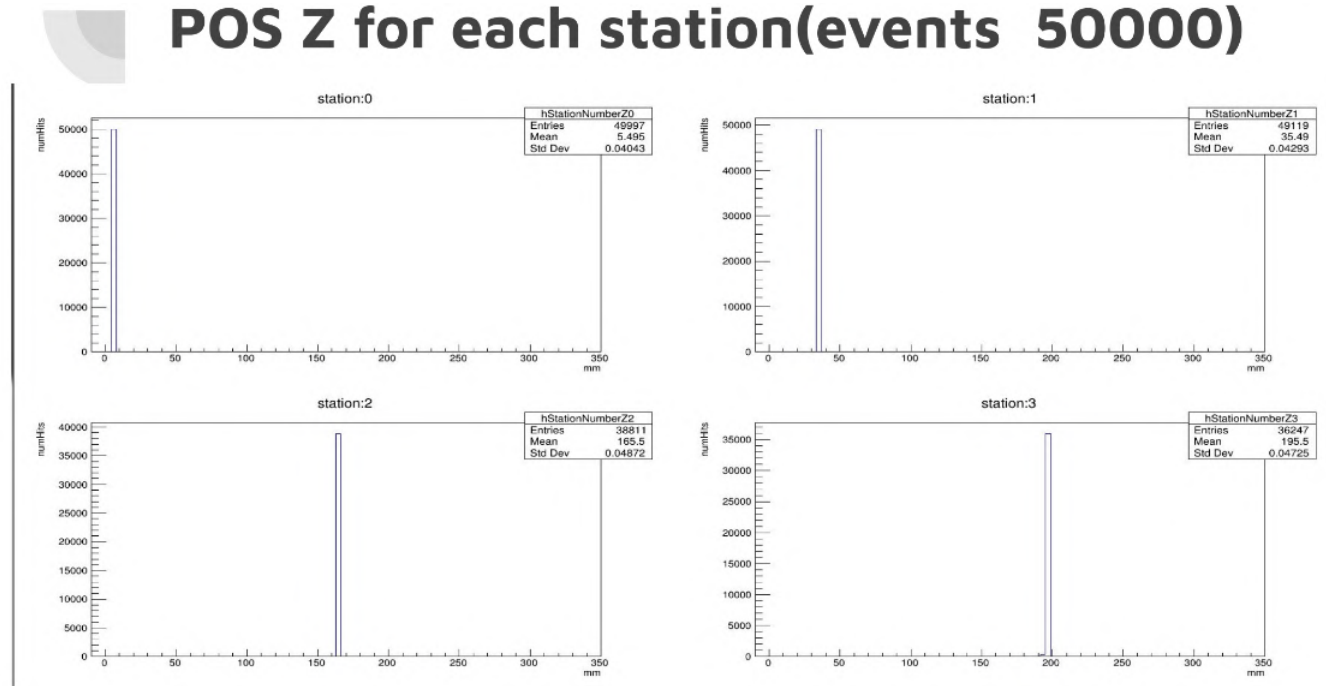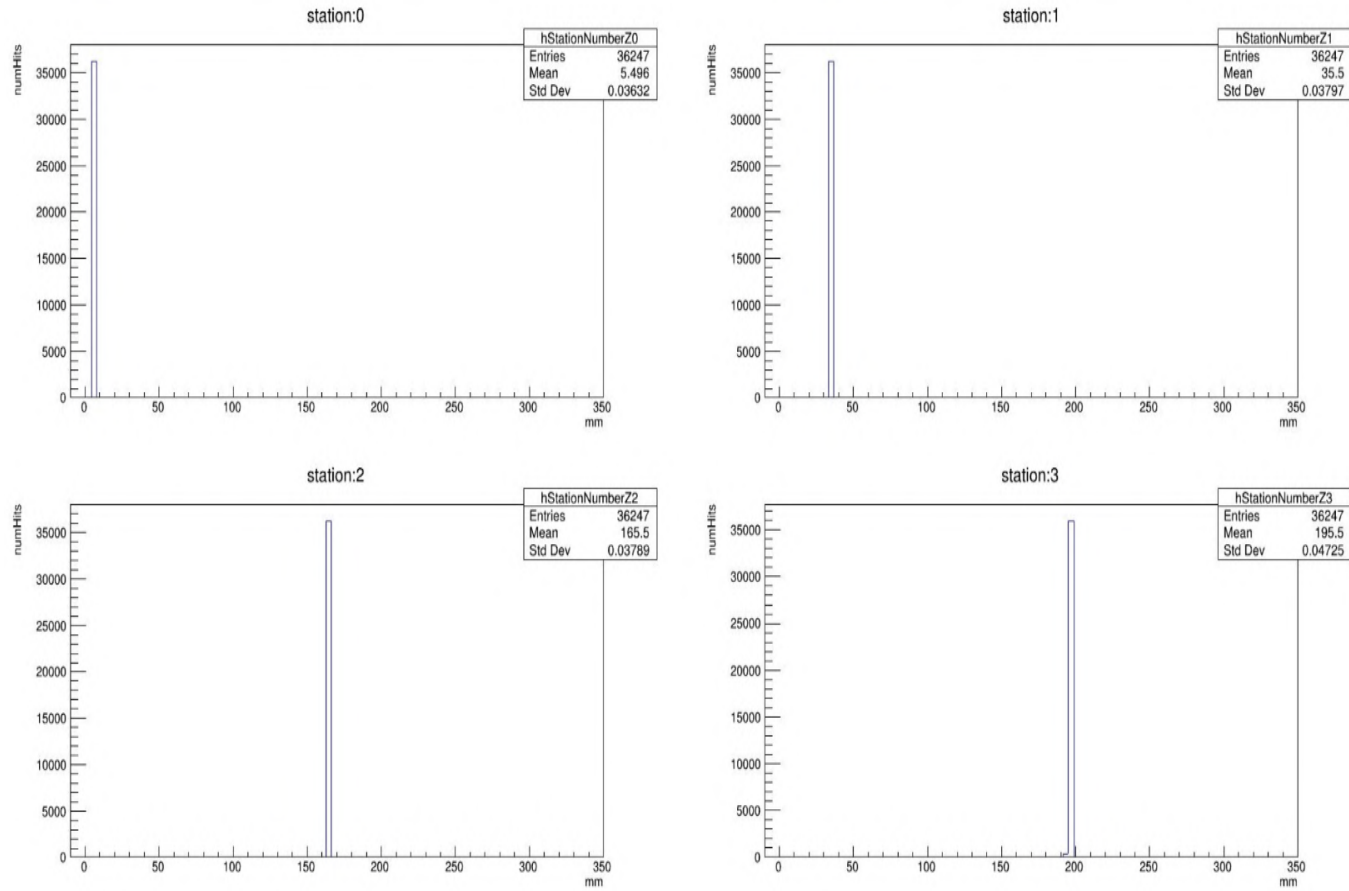
Fig. 5.5 we can see that number of muons is reducing in each layer due to scattering/absorption. However for analysis of tracks we need to consider only those muons which have crossed all the layers

Our study focused on calculating the scattering angles between incoming and outgoing muons. We employed two planar angles, the XZ and YZ angles, for our calculations to achieve this. We obtained the scattering angles by taking the quadratic sum of these angles in the respective planes. Additionally, we computed the standard deviation of the scattering angle distribution using Highland's formula. This approach allowed us to gain valuable insights into the scattering behaviour of muons and provided a helpful characterization of their interactions in our experimental setup.
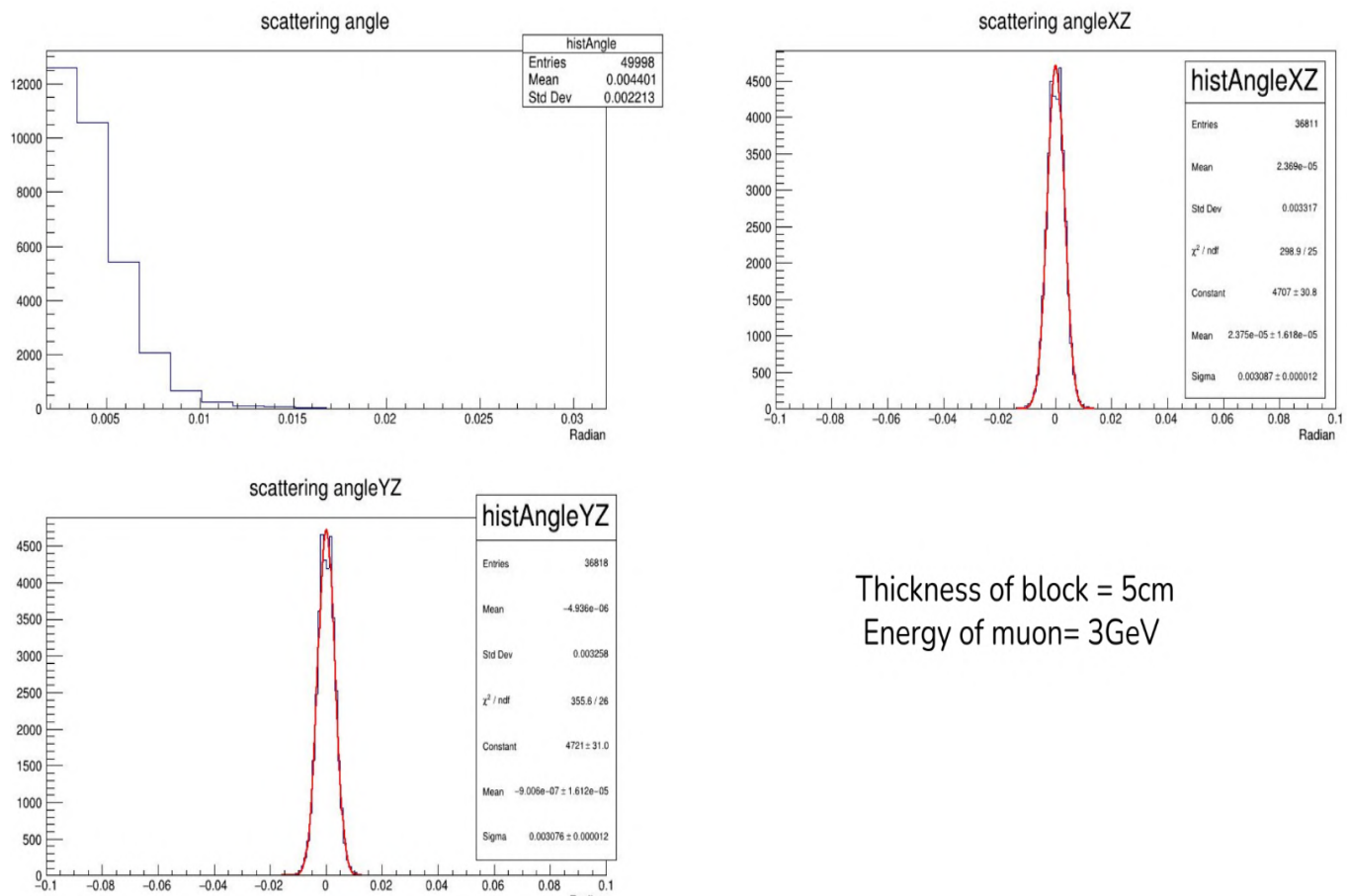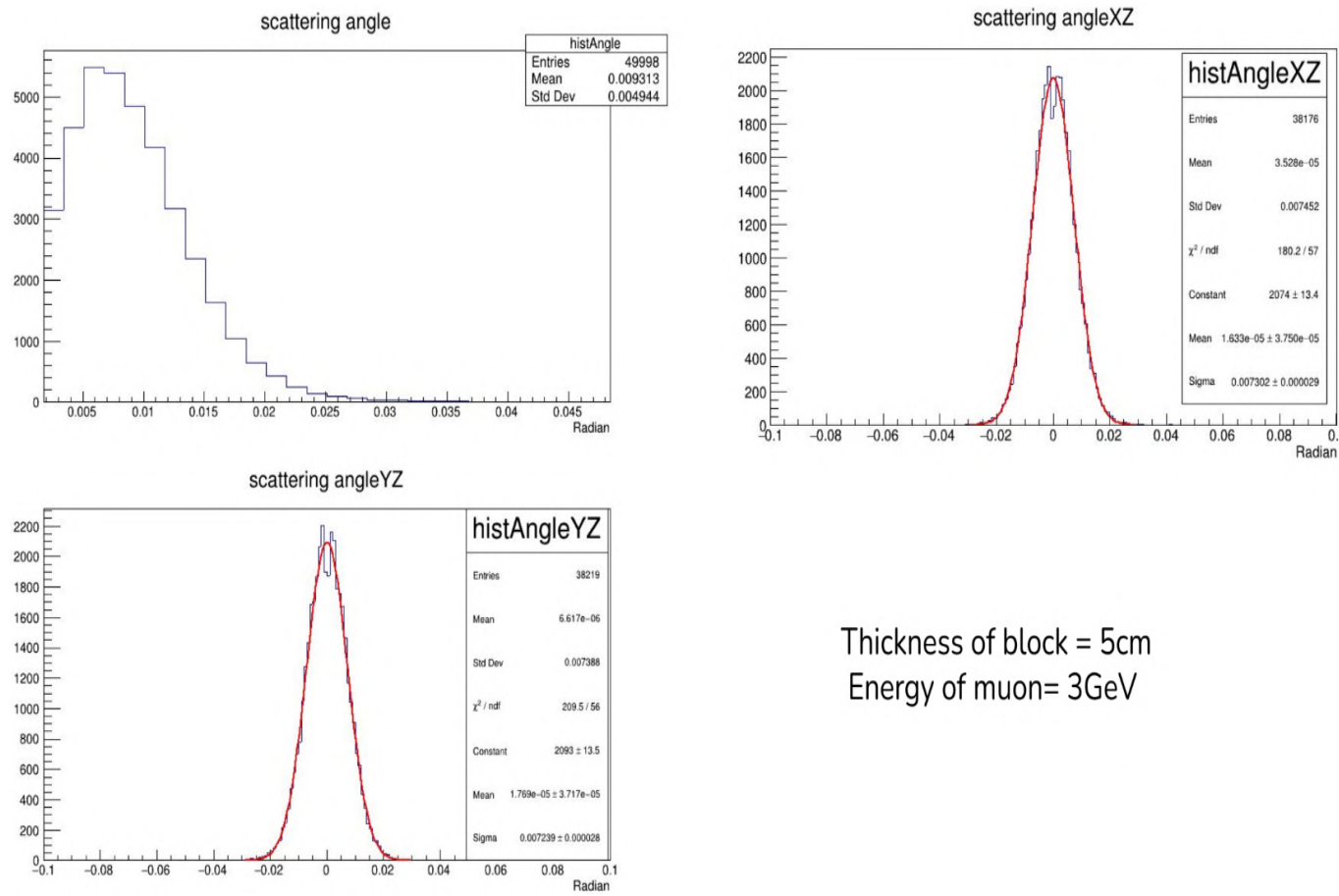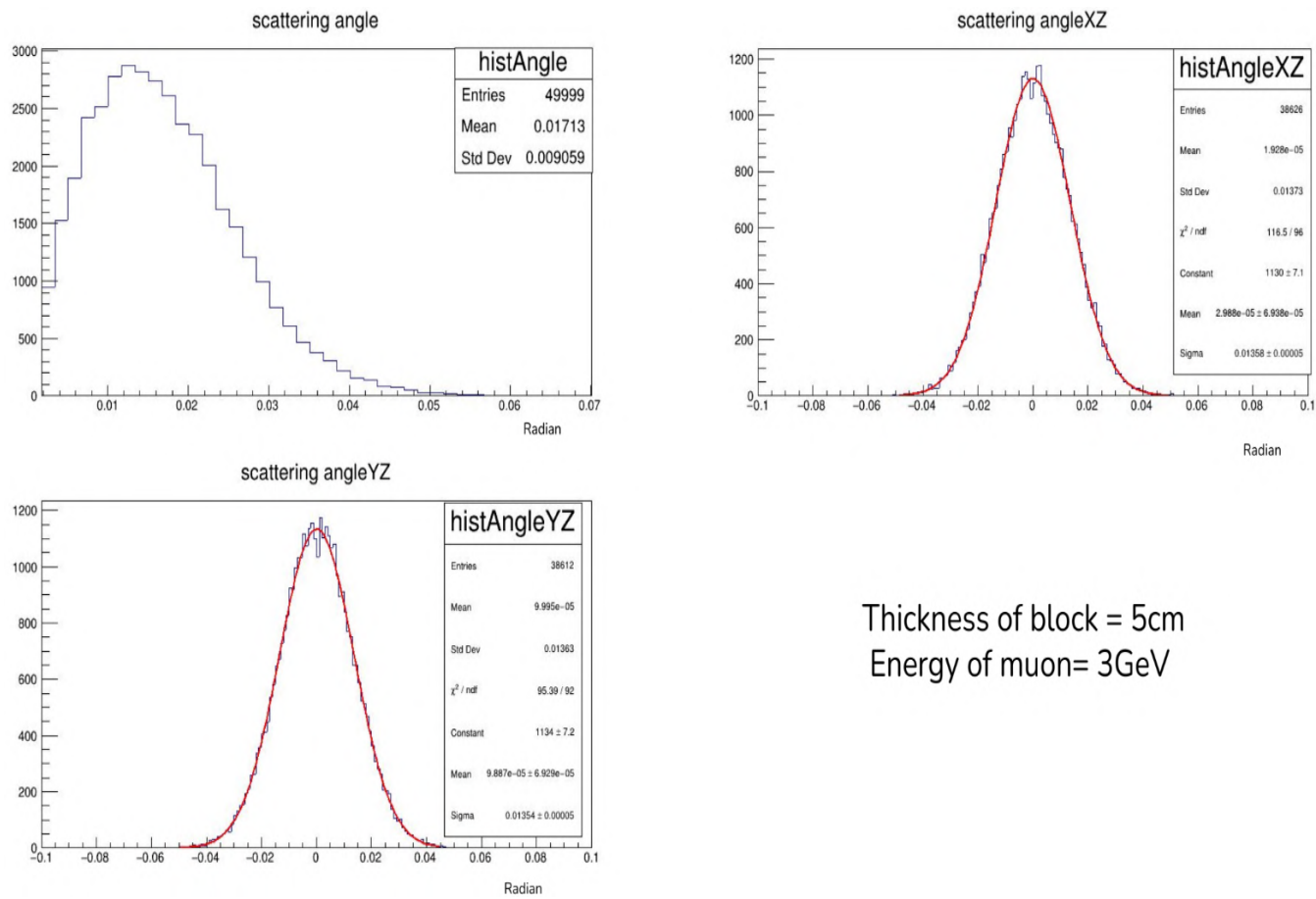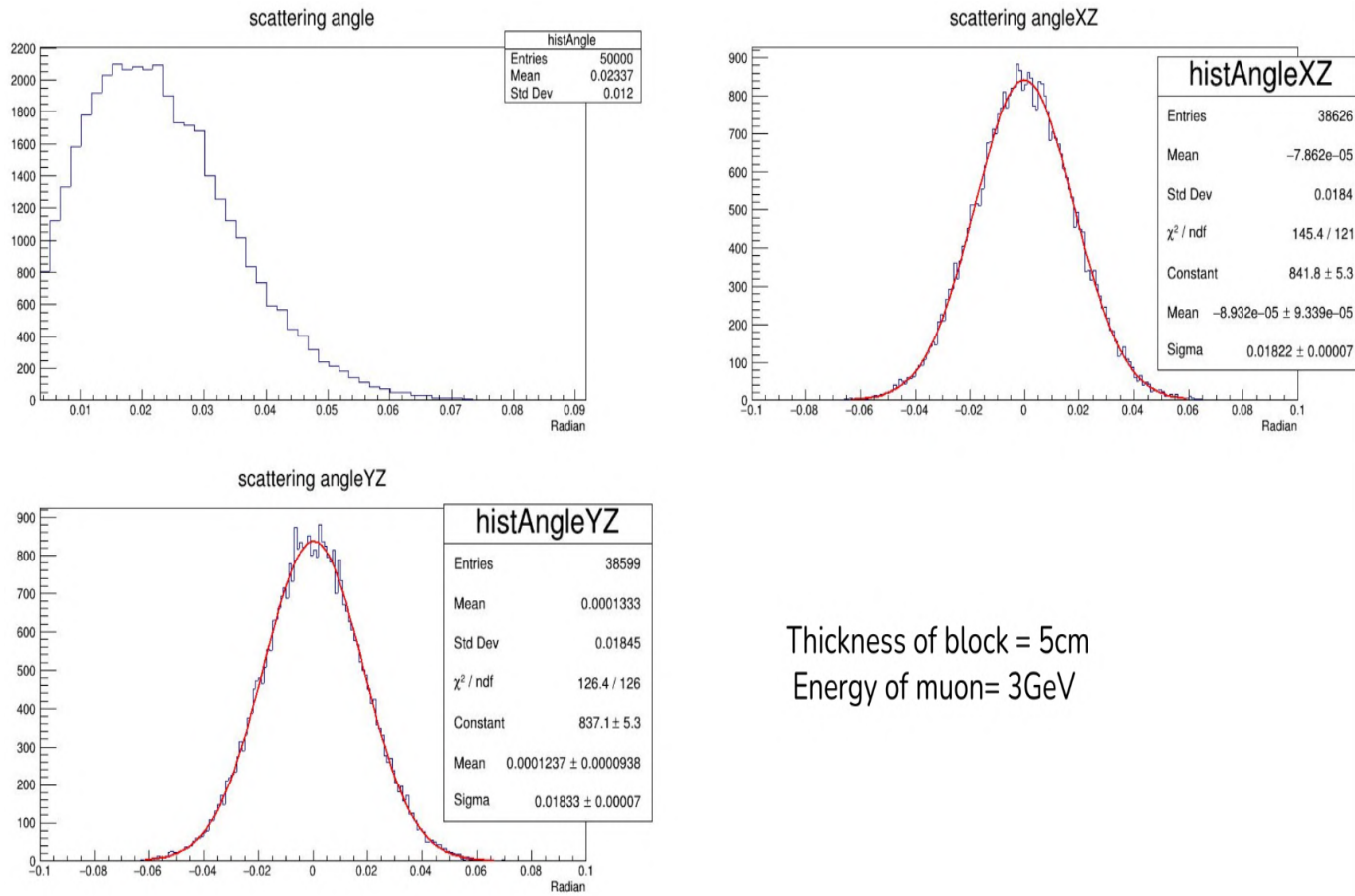
Fig. 5.6 Aluminium

Fig. 5.7 Iron

Fig. 5.8 Lead

Fig. 5.9 Uranium

5.6 POCA Scattering points

The Point of Closest Approach (POCA) [6] algorithm is a mathematical technique
used to determine the mutually closest distance between two skew lines or tracks
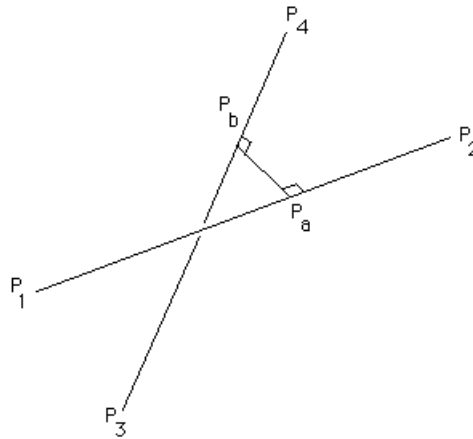moving in three-dimensional space.

Fig. 5.10 Two tracks in 3d space. We need to find the mid-point of the shortest line.

5.6.1 Shortes Line Segment

– 1. The shortest line segment between two lines "a" and "b" can be found
by minimizing the distance function $\|Pb - Pa\|^2$ and solving the resulting
equations for μ_a and μ_b, then substituting these values into the line equations
to obtain the intersection points.

– 2. The shortest line segment between two lines is perpendicular to both
lines. This line segment can be determined by finding the direction vector
of each line and taking their cross-product to get the direction vector of the
shortest line. The point of intersection of this shortest line with one of the
given lines can then be calculated, and it will give the coordinates of the
nearest point on that line.

The dot product equations for finding the shortest line segment between two
lines are:

$$(Pa - Pb) \cdot (P2 - P1) = 0$$
$$(\ Pa - Pb) \cdot (P4 - P3) = 0$$

Expanding these equations with the line equations:

$$(P1 - P3 + \mu a(P2 - P1) - \mu b(P4 - P3)) \cdot (P2 - P1) = 0$$
$$(P1 - P3 + \mu a(P2 - P1) - \mu b(P4 - P3)) \cdot (P4 - P3) = 0$$
$$(P1 - P3) \cdot (P2 - P1) + \mu a(P2 - P1) \cdot (P2 - P1) - \mu b(P4 - P3) \cdot (P2 - P1) = 0$$
$$(P1 - P3) \cdot (P4 - P3) + \mu a(P2 - P1) \cdot (P4 - P3) - \mu b(P4 - P3) \cdot (P4 - P3) = 0$$

The equations for finding μa and μb, which determine the shortest line segment between two lines, are:

$$\mu_a = (d_{1343} \ d_{4321} - d_{1321} \ d_{4343}) / (d_{2121} \ d_{4343} - d_{4321} \ d_{4321})$$
$$\mu_b = (d_{1343} + \mu a * d_{4321}) / d_{4343}$$

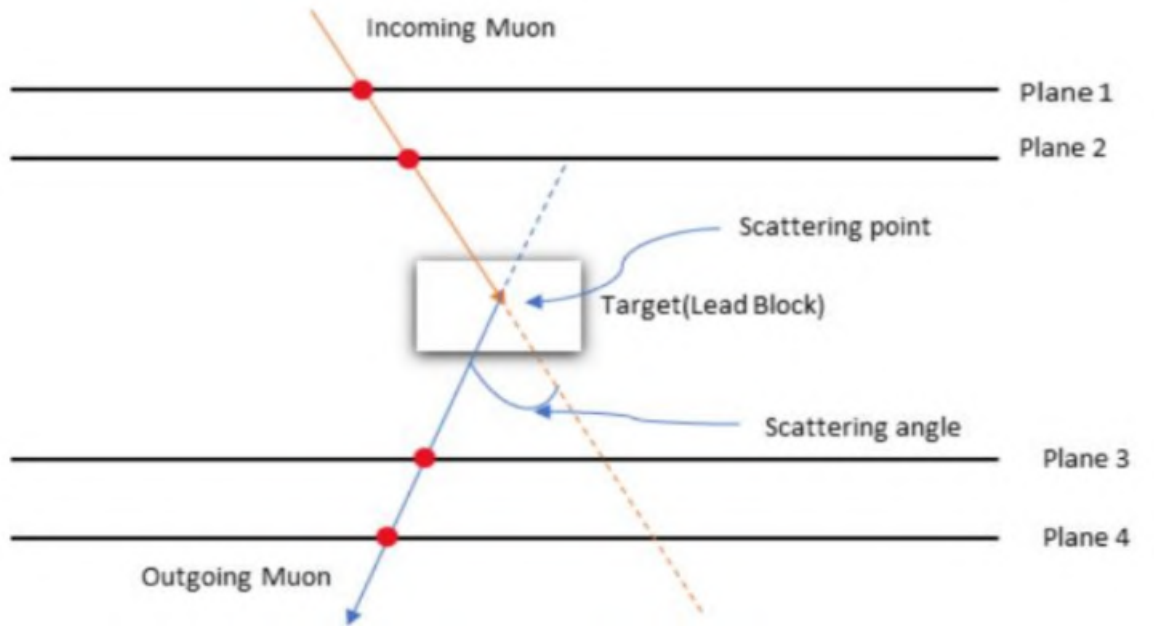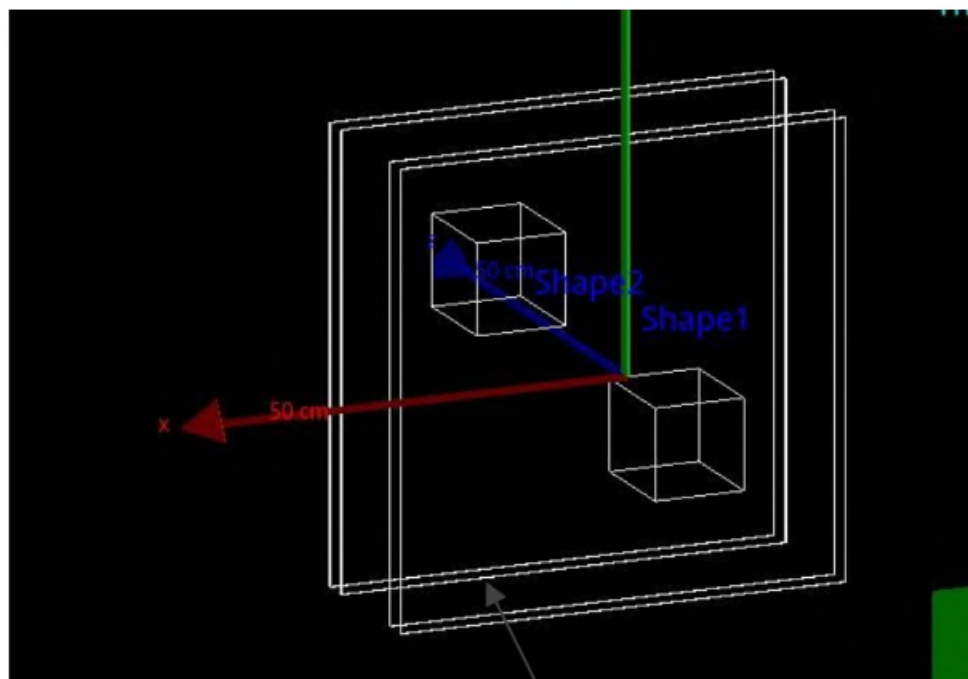where $d_{mnop} = (x_m - x_n)(x_o - x_p) + (y_m - y_n)(y_o - y_p) + (z_m - z_n)(z_o - z_p)$.

Fig. 5.11 Scattering point

Fig. 5.12 Geant4 geometry

Fig. 5.13 Images obtained by plotting scattering points

Input(Muons shower using primary generator)

hits in sensitive layers of detector

storing hits info like momentum, position

saving these parameters in a root file

use MakeClass method to get full control over root file

use more conditional statement like we only consider muons which crossed all four layers

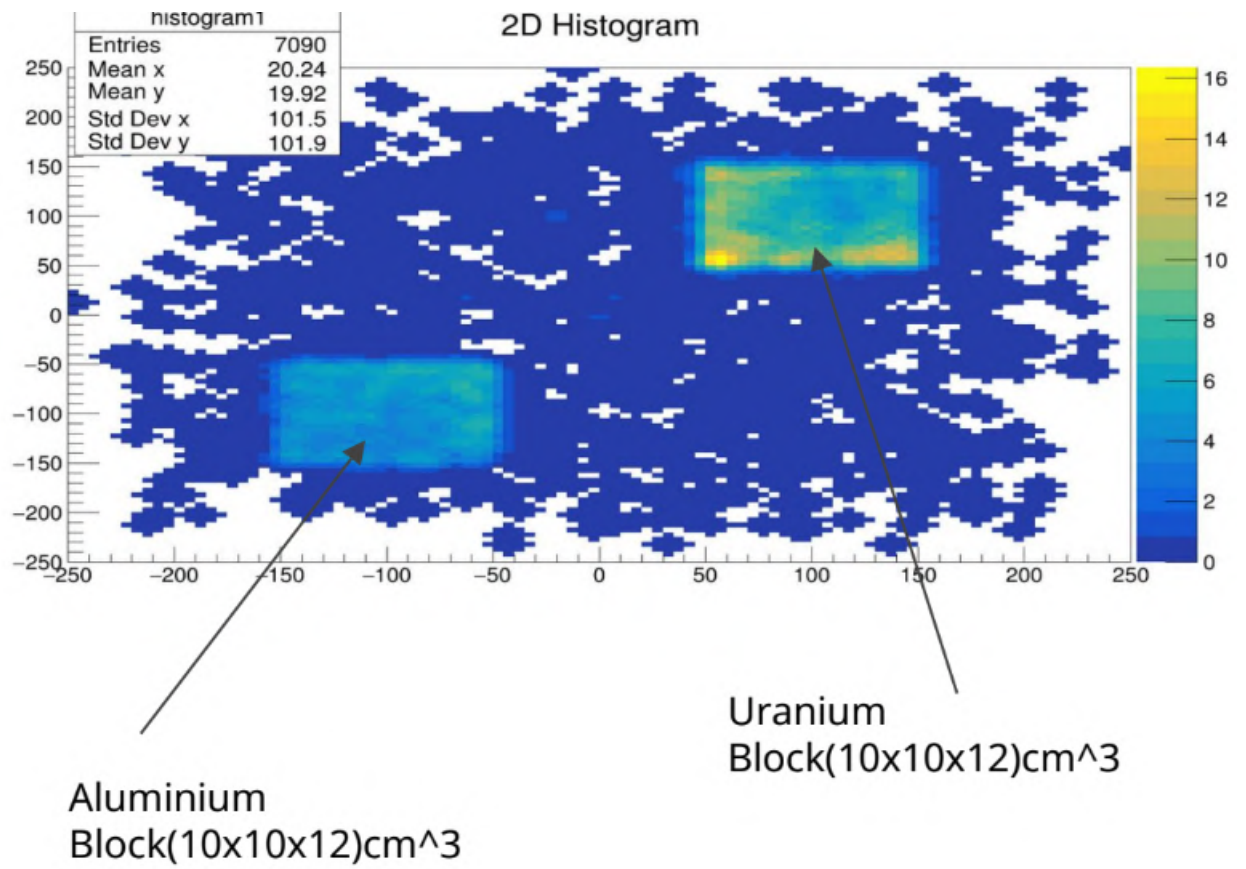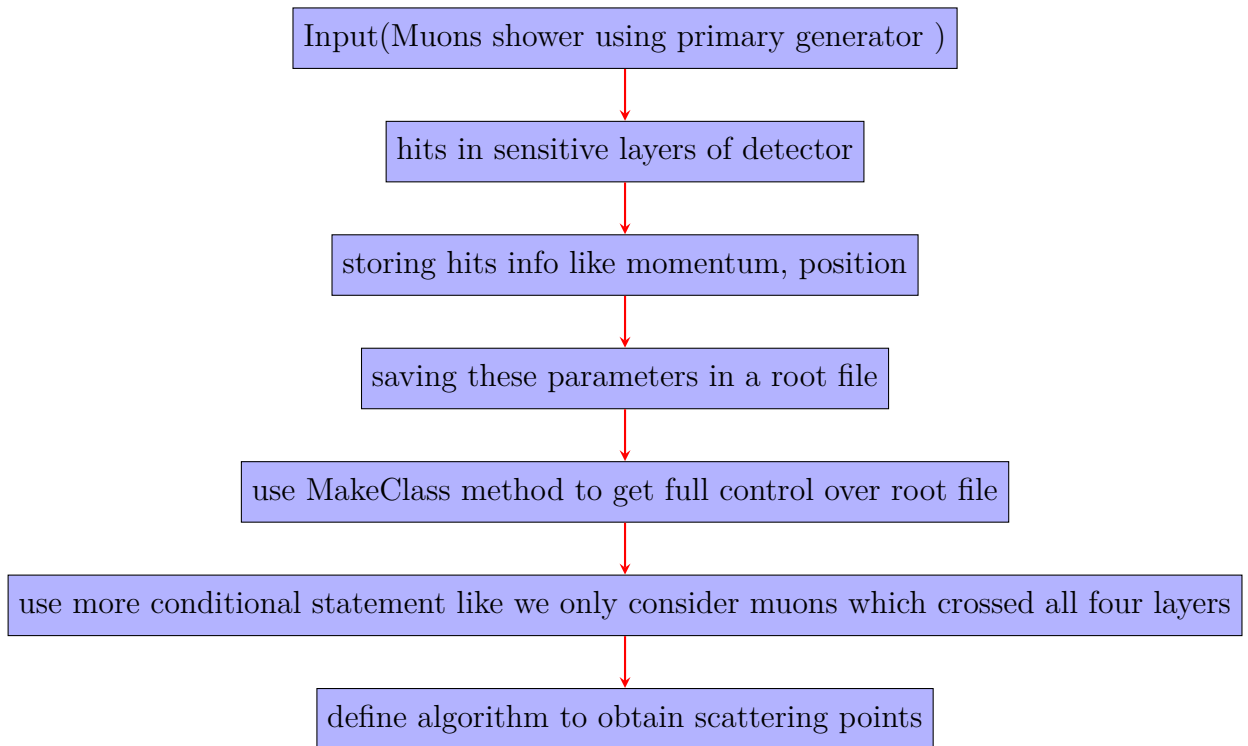define algorithm to obtain scattering points

Fig. 5.14 Summary of steps that were performed to get the image

Chapter 6

Conclusions and Future Scope

In summary, our project involved simulating a basic muoscope setup, achieving two key objectives. The initial accomplishment involved distinguishing materials based on their Z number and then utilizing the POCA algorithm to image various metal blocks. As we move forward, there are other opportunities for project expansion. Firstly, we're actively integrating garfieldpp into our pipeline to gain insights into avalanches and cluster size for more accurate and detailed results. Additionally, there's another way where we can use voxelization to visualize the metal block and generate a more comprehensive and informative image by assigning scattering angles to individual voxels and plotting them.

References

[1] R. Santonico and R. Cardarelli. Development of resistive plate counters. *Nuclear Instruments and Methods in Physics Research*, 187(2):377–380, 1981.

[2] S. Agostinelli, J. Allison, K. Amako, J. Apostolakis, H. Araujo, P. Arce, M. Asai, D. Axen, S. Banerjee, G. Barrand, F. Behner, L. Bellagamba, J. Boudreau, L. Broglia, A. Brunengo, H. Burkhardt, S. Chauvie, J. Chuma, R. Chytracek, G. Cooperman, G. Cosmo, P. Degtyarenko, A. Dell'Acqua, G. Depaola, D. Dietrich, R. Enami, A. Feliciello, C. Ferguson, H. Fesefeldt, G. Folger, F. Foppiano, A. Forti, S. Garelli, S. Giani, R. Giannitrapani, D. Gibin, J.J. Gómez Cadenas, I. González, G. Gracia Abril, G. Greeniaus, W. Greiner, V. Grichine, A. Grossheim, S. Guatelli, P. Gumplinger, R. Hamatsu, K. Hashimoto, H. Hasui, A. Heikkinen, A. Howard, V. Ivanchenko, A. Johnson, F.W. Jones, J. Kallenbach, N. Kanaya, M. Kawabata, Y. Kawabata, M. Kawaguti, S. Kelner, P. Kent, A. Kimura, T. Kodama, R. Kokoulin, M. Kossov, H. Kurashige, E. Lamanna, T. Lampén, V. Lara, V. Lefebure, F. Lei, M. Liendl, W. Lockman, F. Longo, S. Magni, M. Maire, E. Medernach, K. Minamimoto, P. Mora de Freitas, Y. Morita, K. Murakami, M. Nagamatu, R. Nartallo, P. Nieminen, T. Nishimura, K. Ohtsubo, M. Okamura, S. O'Neale, Y. Oohata, K. Paech, J. Perl, A. Pfeiffer, M.G. Pia, F. Ranjard, A. Rybin, S. Sadilov, E. Di Salvo, G. Santin, T. Sasaki, N. Savvas, Y. Sawada, S. Scherer, S. Sei, V. Sirotenko, D. Smith, N. Starkov, H. Stoecker, J. Sulkimo, M. Takahata, S. Tanaka, E. Tcherniaev, E. Safai Tehrani, M. Tropeano, P. Truscott, H. Uno, L. Urban, P. Urban, M. Verderi, A. Walkden, W. Wander, H. Weber, J.P. Wellisch, T. Wenaus, D.C. Williams, D. Wright, T. Yamada, H. Yoshida, and D. Zschiesche. Geant4—a simulation toolkit. *Nuclear Instruments and Methods in Physics Research Section A: Accelerators, Spectrometers, Detectors and Associated Equipment*, 506(3):250–303, 2003.

[3] National Institute of Standards and Technology. Security requirements for cryptographic modules. Technical Report Federal Information Processing Standards Publications (FIPS PUBS) 140-2, Change Notice 2 December 03, 2002, U.S. Department of Commerce, Washington, D.C., 2001.

[4] D Pagano, G Bonomi, A Donzella, A Zenoni, G Zumerle, and N Zurlo. EcoMug: An efficient COsmic MUon generator for cosmic-ray muon applications. *Nucl. Instrum. Methods Phys. Res. A*, 1014(165732):165732, October 2021.

[5] Rene Brun, Fons Rademakers, Philippe Canal, Axel Naumann, Olivier Couet, Lorenzo Moneta, Vassil Vassilev, Sergey Linev, Danilo Piparo, Gerardo GANIS, Bertrand Bellenot, Enrico Guiraud, Guilherme Amadio, wverkerke, Pere Mato, TimurP, Matevž Tadel, wlav, Enric Tejedor, Jakob Blomer, Andrei Gheata, Stephan Hageboeck, Stefan Roiser, marsupial, Stefan Wunsch, Oksana Shadura, Anirudha Bose, CristinaCristescu, Xavier Valls, and Raphael Isemann. root-project/root: v6.18/02, June 2020.

[6] Paul Bourke. Geometry in computer graphics - point, line, plane, October 1988. Accessed: November 14th, 2023.